

ARTICLE OPEN



Climatological Madden-Julian Oscillation during boreal spring leads to abrupt Australian monsoon retreat and Asian monsoon onsets

Bin Wang¹✉, Lun Dai¹✉, Tat Fan Cheng^{1,2}, Sun-Seon Lee^{3,4}, Tianyi Wang⁵ and Chunhan Jin⁶

Abrupt monsoon onsets/retreats are indispensable targets for climate prediction and future projection, but the origins of their abruptness remain elusive. This study establishes the existence of three climatological Madden-Julian Oscillation (CMJO) episodes contributing to the rapid Australian summer monsoon retreat in mid-March, the South China Sea (or East Asian) summer monsoon onset in mid-May, and the Indian summer monsoon onset in early June. The CMJO displays a dynamically coherent convection-circulation structure resembling its transitional counterpart, demonstrating its robustness as a convectively coupled circulation system and the tendency of the transient MJOs' phase-lock to the annual cycle. The CMJO is inactive during the boreal winter due to destructive year-to-year modulations of El Niño-Southern Oscillation. We hypothesize that the interaction between atmospheric internal variability (MJO) and the insolation-forced slow annual cycle generates the sudden monsoon withdrawal/onset during the boreal spring. Understanding the factors determining the timing and location of the MJO's phase-locking and its variability is vital for monsoon forecasting and climate projection.

npj Climate and Atmospheric Science (2024)7:40; <https://doi.org/10.1038/s41612-024-00566-9>

INTRODUCTION

Monsoon is essentially a response of the coupled atmosphere-land-ocean climate system to the annual variation of solar radiation¹. While the solar forcing exhibits a “smoothed” annual variation at any given latitude, the monsoonal response displays substantial departures from a smoothed (or slow) annual cycle. The significant departures from their normal seasonal mean values on or near a particular calendar date are often called “climate singularities”^{2,3}. Similarly, a “monsoon singularity” refers to a monsoon weather event that occurs on or near a fixed calendar day or calendar pentad with usual regularity⁴. Examples are the abrupt onset of the South China Sea (SCS) summer monsoon in Pentad 28 (hereafter abbreviated P28; May 16–20) and the sudden onset of the Indian Summer Monsoon (ISM) in Kerala during P31 (May 31–June 4)⁵. Improving the understanding of the sudden changes and monsoon singularities in the annual cycle has profound implications for the seasonal forecasts and climate projections, as socio-economic activities, including agricultural planning and disaster mitigation, demand accurate monsoon onset and withdrawal predictions both presently and in the future.

Wang and Xu (1997)⁶ (hereafter WX97) found that transient intraseasonal oscillation (ISO) tends to occur at some particular times of the year, resulting in significant and phase-locked ISO in the mean climatological annual variation. This phenomenon is termed Climatological ISO (CISO), whose propagation connects summer monsoon singularities at various places, offering a dynamic interpretation of the boreal summer monsoon singularity. ISO in the boreal summer distinguishes from the equatorial eastward propagating Madden-Julian Oscillation (MJO)⁷ that prevails in the boreal winter by its prominent northward propagation and off-equatorial maximum variability centers. Thus,

the term “boreal summer ISO” (BSISO) was coined⁸, and a model was developed to explain why the BSISO propagates northward and why its variability is confined in the monsoon region of high moist static energy and easterly vertical wind shears⁸. Over the Indian monsoon region, the dominant northward propagating ISO was also called a monsoonal ISO⁹.

The summertime monsoonal CISO has been widely recognized to shape the monsoon onsets and retreats in East Asia, WNP, and South Asia (e.g., Ref. 10–18). For instance, the climatological northward migration of the East Asian (EA) rain bands can be explained by a northward propagating CISO event^{10,17}. Daily atmospheric diabatic heating and sea surface temperature (SST) in the WNP might be important factors in maintaining the CISO related to the EA summer monsoon (EASM)¹⁶. The leading mode of zonal wind CISO in the mid-upper troposphere was linked to the convection over southeastern China and the WNP¹⁸. So far, CISO studies have been primarily focused on the boreal summer, and the term CISO primarily links to climatological BSISO.

The tropical ISO has been recognized to comprise two modes: the equatorial eastward propagating MJO mode that prevails from December to April and the BSISO mode that dominates from June to October¹⁹. May and November are transitional months when the predominant mode changes from one to the other. As shown shortly, while the ISOs during May have a prominent northward propagation component, they also demonstrate a significant eastward propagation along the equator. For this reason, in this work, we refer to the tropical, large-scale eastward propagating ISO from December to May as the MJO.

Thus far, little has been known concerning the potential phase lock of MJO to the annual cycle, leaving a gap of knowledge to be filled. Here we aspire to address the following questions: Does

¹Department of Atmospheric Sciences, International Pacific Research Center and Atmosphere-Ocean Research Center, University of Hawaii at Manoa, Honolulu, HI, USA.

²Department of Civil and Environmental Engineering, The Hong Kong University of Science and Technology, Clear Water Bay, Hong Kong, China. ³Center for Climate Physics, Institute for Basic Science (IBS), Busan, Republic of Korea. ⁴Pusan National University, Busan, Republic of Korea. ⁵Marine Science and Technology College, Zhejiang Ocean University, Zhoushan, China. ⁶College of Geography and Remote Sensing Science, Xinjiang University, Urumqi 830017, China. ✉email: wangbin@hawaii.edu; dailun@hawaii.edu

MJO propagation phase-lock to the annual cycle over the equatorial regions? Are there any statistically significant and physically meaningful “Climatological MJO” (CMJO) signals during the boreal winter and spring? If the CMJO signals exist, what are their dynamic and thermodynamic structure and propagation features? Could the CMJO signals link to the Asian-Australian monsoon’s sudden changes?

In alignment with the afore-listed questions, we investigate the pentad-mean annual cycle averaged in the past 42 years (1979–2020), focusing on detecting the CMJO signals from March to May and their linkages with the monsoon singularities. These climatological means were computed based on a longer period of data than the early CISO studies^{10,11,13,14}. In the following, we first depict the sudden Australian monsoon retreat and the abrupt Asian monsoon onsets in the SCS and Southern India. We then explore the CISO seasonality and identify three crucial CMJO episodes. We also explore how the three CMJO episodes shape the sudden changes in the transition from the Australian summer monsoon to the Asian summer monsoon. Lastly, we elucidate the coherent dynamic structure and propagation mechanism of the CMJO.

RESULTS

Sudden Australian monsoon retreat and abrupt Asian monsoon onsets

Circulation indices based on the 850-hPa winds have been widely proposed to monitor monsoon seasonal variation and climate variability^{20–24}. To cope with the evolution of the CMJO, here we offer three indices based on outgoing longwave radiation (OLR; a proxy for precipitation) to represent the seasonal cycles of the regional monsoons (Fig. 1). The first index is an OLR Indonesian-Australian monsoon index averaged over (15°S–5°S, 120°E–150°E) (Fig. 1a), which corresponds well to the broad-scale Australian monsoon circulation index (i.e., 850-hPa zonal wind averaged over 15°S–5°S, 110°E–130°E)²⁵. The second one is an OLR SCS summer monsoon onset index averaged over the northern SCS (10°N–20°N, 110°E–120°E), which is highly correlated with the 850-hPa zonal wind index averaged over the central SCS (5°N–15°N, 110°E–120°E)⁴. Likewise, monsoon onset over Kerala (MOK) has been considered the commencement of the Indian principal rainy season. The OLR averaged over (5°N–15°N, 60°E–80°E) was taken as a measure of the intensity of deep convection near the southern tip of India (including Kerala) and the southeastern Arabian Sea, which agreeably matches MOK and the southwest monsoon onset over the Arabian Sea²⁶.

With the three proposed OLR indices at hand, we can disentangle the CISO signals from their slow annual cycles at the three regional monsoon locations. The Indonesian-Australian monsoon features a sudden increase of OLR in mid-March, which implies abruptly suppressed convection and thereby signifies a hasty retreat of the Indonesian-Australian summer monsoon (Fig. 1a, c). The retreat links to a significant local CISO signal in March, with the driest phase from P16 to P18 (March 17–31) (Fig. 1b). The SCS summer monsoon shows a surge of rainfall (in tandem with a decline in OLR) in mid-late May, which corresponds to a significant local CISO peak wet phase in P28 and P29 (May 16–25) (Fig. 1d–f). The ISM onset is most spectacular at the beginning of June, as manifested by a pluvial peak in P31 and P32 (Fig. 1g, h). Both the slow annual cycle and the CISO contribute to the abrupt retreat/onset. The slow annual cycle, consisting of the first four harmonics, features a rapid transition during the retreat/onset periods. However, the CISO makes the onset/retreat more abrupt and advances the date determined by the slow annual cycle by one to two pentads (Fig. 1b, e, h).

Interestingly, the extreme wet-dry phases at the three remote locations appear teleconnected. From P16 to P18, when the

Australian monsoon retreats (Fig. 1a), the SCS experiences a peak wet phase (Fig. 1d), indicating a cross-hemispheric linkage of the Australian monsoon withdrawal with enhanced EA tropical monsoon activity. During P28 and P29, when the SCS summer monsoon starts, the Australian monsoon experiences a dry phase, confirming the meridional linkage. In addition, the Indian monsoon is prone to a pre-monsoon compound hazard of drought and heatwaves²⁷ (Fig. 1d, g), suggesting an out-of-phase relationship of the subseasonal climate variation between southwest India and the northern SCS. Concomitant with the ISM outbreak in P31, the Australian and SCS monsoon regions experience a dry phase (Fig. 1a, d, g). These wet-dry teleconnections across the three far-apart monsoon locations bespeak the necessity of investigating the CISO propagation in the entire Asian-Australian and warm pool regions during the boreal spring, which is also the Asian-Australian transition period.

CISO seasonality and three boreal spring CMJO episodes

CISO, like its transient counterpart, exhibits salient seasonality (Fig. 2). Notably, the standard deviation of the OLR CISO is the largest in the boreal summer but remain the lowest in the boreal winter, inferring that climatological BSISO is substantially stronger than the CMJO. CISO’s intraseasonal variability center shifts from the Southern Hemisphere in the boreal winter from December to February (DJF) to the Northern Hemisphere in the boreal summer from June to August (JJA) (Fig. 2b, d). During transition seasons, namely, March–April–May (MAM) and September–October–November (SON) (Fig. 2a, c), the CISO variability is confined to the tropical region between 15°S and 25°N, slightly biased to the northern tropics. However, the CISO variability displays a notable spring–fall asymmetry, whereby its intensity is more intensive in the boreal spring than in the boreal fall. Overall, boreal spring is an active season for CISO.

From March to May, three significant equatorial CMJO episodes propagate eastward over the Maritime Continent and the western Pacific (Fig. 3). The first episode occurs in mid-March when a short-lived but significantly dry signal migrates eastward over the Maritime Continent. The second is a wet episode propagating eastward in early May over the equatorial western Pacific from 120°E to 160°E. The third is a dry episode in May, originating at 90°E and propagating eastward to 160°E. As revealed later, the two CMJO episodes in May also exhibit prominent northward or northeastward propagations over the SCS and the northern Indian Ocean, respectively.

The inactive CMJO activity during the boreal winter is one of the major findings in this study. Transient MJO activity along the equator is prominent during the boreal winter²⁸, but why does the wintertime CMJO appear inactive (Fig. 3a)? We conjecture that the pronounced interannual variability of MJO prohibits its phase locking to the annual cycle. El Niño–Southern Oscillation (ENSO) generally exhibits the maximum amplitude in the boreal winter²⁹ due to the seasonal variation of the western Pacific surface winds³⁰. During the mature phase of El Niño events, the MJO activity markedly shifts eastward into the central Pacific³¹. El Niño favors a fast eastward propagation event that shifts the variability to the central Pacific, while La Niña favors the standing events wherein the anomalous convection is confined to the Indian Ocean^{31,32}. Thus, ENSO could cause a sizable year-to-year variability of transitional MJO events, destructive to the CMJO formation during the boreal winter.

To test the destructive effect of ENSO on the CMJO, here we compared the mean CMJOs derived from 24 neutral years with that from 18 ENSO years (Fig. 4a). Evidently, the CMJO is prominent during the neutral years but remains inactive during ENSO years (Fig. 4c, d). This finding confirms that the ENSO has destructive effects on the transient MJO’s phase lock to the annual cycle, or CMJO. It also suggests that the CMJO might become more significant in an epoch of weak ENSO.

Indonesian-Australian monsoon index

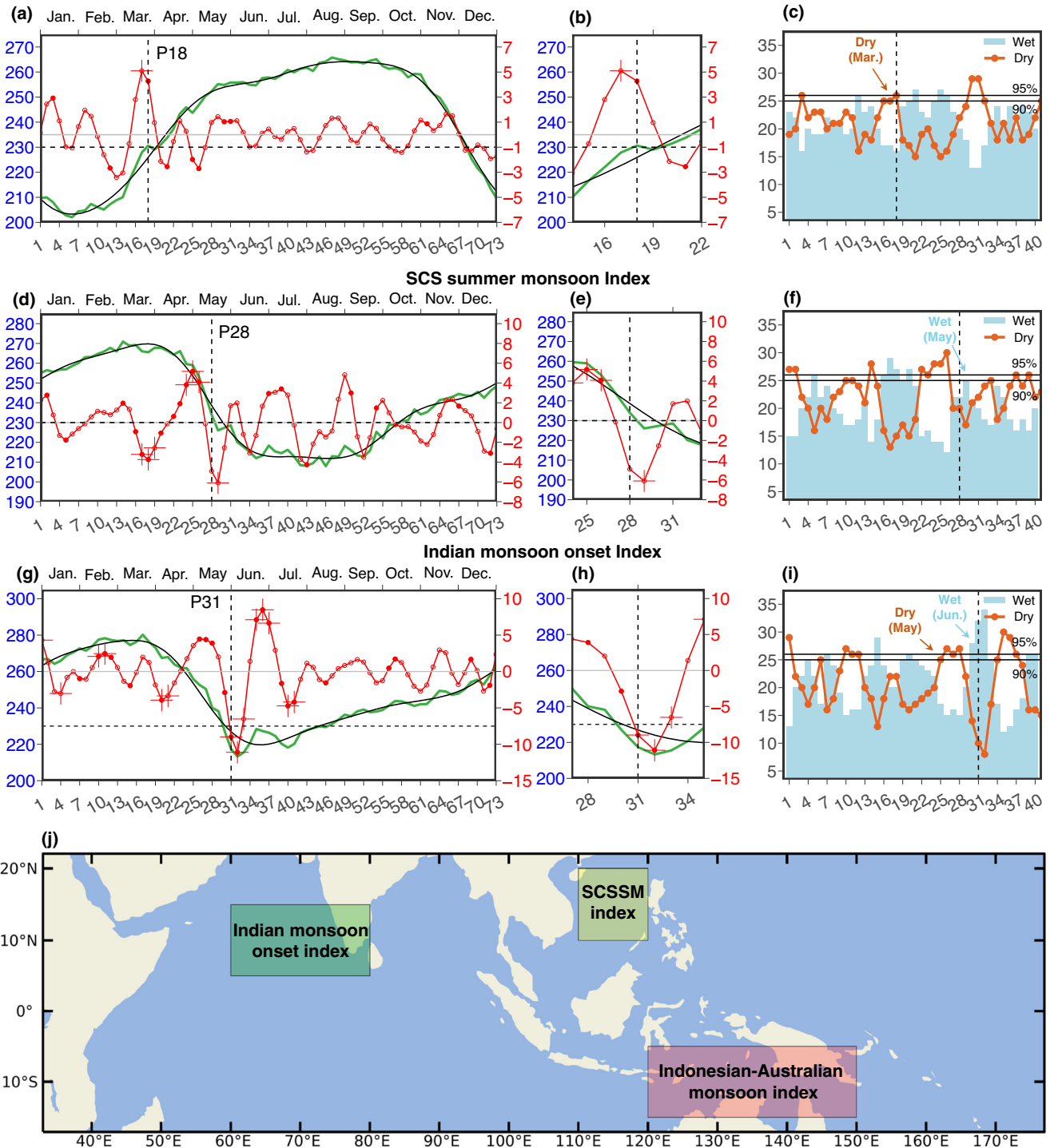


Fig. 1 Abrupt Australian summer monsoon withdrawal (upper panels), and onset of South China Sea (middle panels) and Indian summer monsoon (lower panels). The dashed black lines indicate the corresponding retreat/onset dates (e.g., Ref. 4,5,25). **a** The pentad-mean time series of the Indonesian-Australian monsoon index (green) (i.e., OLR averaged over 15°S–5°S, 120°E–150°E) and the corresponding slow annual cycle (black) and CISO (red) in units of $W m^{-2}$ derived from 42-year data. The solid red dot (cross) indicates significant CISO by the A/S (sign) test at the 95% confidence level. **b** A zoom-in view of the retreat period. **c** Occurrence number of the wet (blue bar) and dry (red curve) phases of CISO. The 95% and 90% confidence levels are indicated by the black horizontal lines. Panels **(d–f)**: As in **a–c** but for the SCS summer monsoon onset index (i.e., OLR averaged over 10°N–20°N, 110°E–120°E). Panels **(g–i)**: As in **a–c** but for the Indian monsoon onset index (i.e., OLR averaged over 5°N–15°N, 60°E–80°E). **j** Geographic regions where the three OLR monsoon indices are defined. SCSSM stands for South China Sea Summer Monsoon.

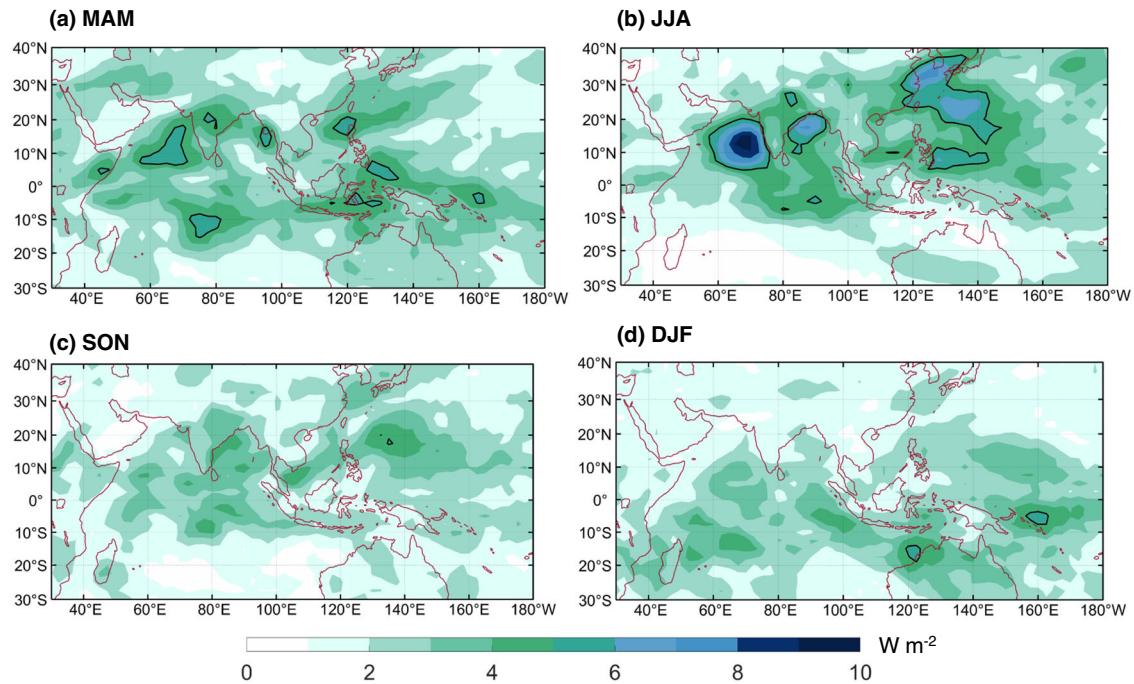


Fig. 2 Seasonal OLR CISO intraseasonal standard deviation. (shading, unit: W m^{-2}) computed from pentad OLR CISO time series during (a) March–April–May (MAM), (b) June–July–August (JJA), (c) September–October–November (SON), and (d) December–January–February (DJF).

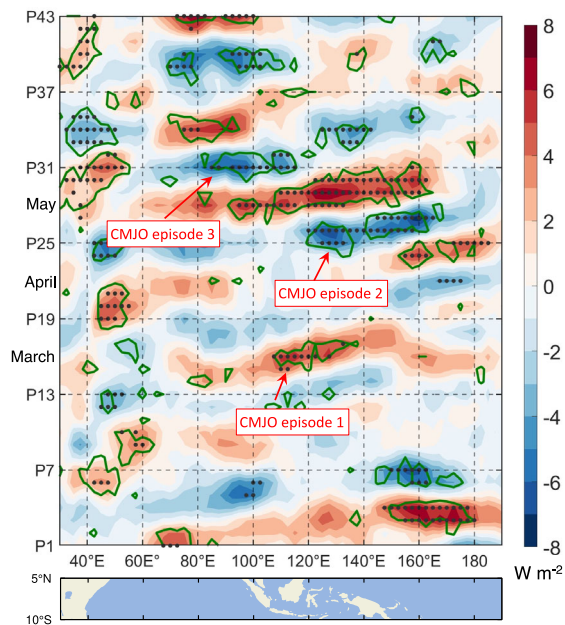


Fig. 3 The CMJO's eastward propagation along the equator. The longitude–time cross sections of the CMJO OLR (units in W m^{-2}) averaged between 10°S and 5°N . The green contour (gray dot) indicates a significant CMJO by the A/S (sign) test at the 95% confidence level. The geographic map on the bottom displays the region where the variables are averaged. The annotated arrows highlight the wet and dry phases discussed in the text.

The March CMJO dry anomalies and the Australian summer monsoon retreat

A notably dry CMJO signal first emerges in 80°E – 90°E and 10°S –EQ in early March (P14) (Fig. 5a). From P15 to P18, the dry CMJO anomalies propagate eastward from the central Indian Ocean

through the Maritime Continent, reaching northern Australia and dissipating afterward (Fig. 5b–f), suggesting a regular occurrence of dry phases causing the Australian monsoon retreat. Thus, the climatological Australian summer monsoon retreat in March^{25,33} is associated with a significant CMJO episode. In contrast, the Australian summer monsoon onset tends to be less abrupt than its withdrawal. The onset in December is often associated with a wet phase of the transitory MJO³⁴, which is not significantly phase-locked to the annual cycle due to the prominent year-to-year influence from ENSO²⁵.

The March CMJO shows dynamically consistent structures between convection and circulation anomalies along the equator (see the lower panels in Fig. 5). The subdued convection consistently evolves with the low-level easterly anomalies underneath and to its west. The 850-hPa minimum specific humidity tends to lead the peak dry phase of CMJO, suggesting that the moisture divergence-induced boundary layer drying is critical to the eastward propagation of CMJO dry phase. The crucial importance of the boundary layer dynamics in driving MJO's eastward propagation has been the core concept of the trio-interaction (convection-dynamics-moisture) theory³⁵.

The early-mid May and the SCS summer monsoon onset

ISOs of different characteristics emerge over the western Pacific and Indian Ocean^{36,37}. Figure 6 shows how a May CMJO triggers monsoon onset over the SCS from P24 (April 26–30) to P28 (May 16–20). Between P24 and P25 (Fig. 6a, b), a significant wet phase develops over Indonesia. Between P26 and P27 (Fig. 6c, d), the convective anomaly intensifies abruptly east of Borneo and subsequently splits into two—one marching eastward to the western Pacific (160°E) while another migrating north-northwestward toward the northern SCS (Fig. 6f). The equatorial eastward propagation in longitudes of 120°E to 160°E in May is well captured in Fig. 3. The northwestward propagating wet anomaly reaches the northern SCS (10°N – 20°N) in P28 (Fig. 6e). During that time, the 850-hPa zonal winds over the central SCS (5°N – 15°N) switch from easterly to westerly, signifying the SCS summer monsoon onset^{38,39}. Taken together, the convective and

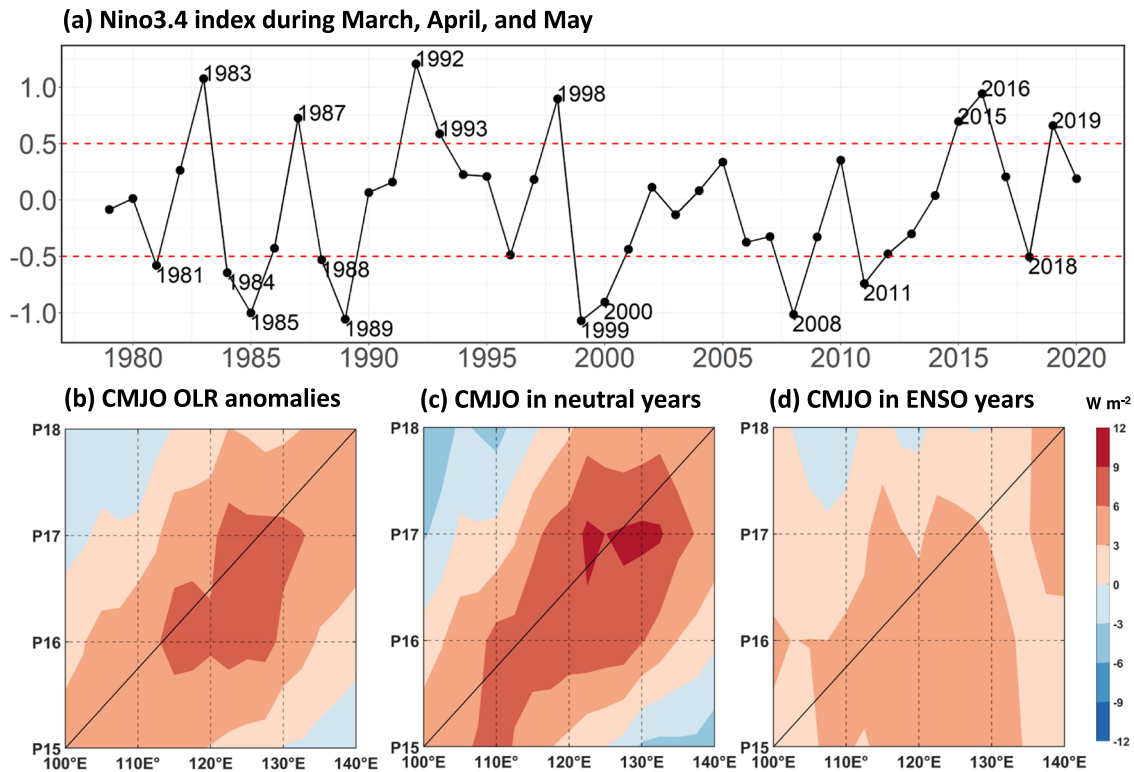


Fig. 4 ENSO weakens climatological MJO. Longitude-time diagram of intraseasonal OLR anomalies during March from P15 to P18. The OLR anomalies in the longitude-time diagram averaged between the equator and 10 S. **a** Time series of Niño 3.4 index during March–April–May. El Niño and La Niña years were defined by values greater than 0.5 °C and less than −0.5 °C, respectively. There are 18 ENSO years and 24 neutral years. **b** Climatological MJO averaged for the 42 years. **c** Same as in **b** but for the 24 neutral years. **d** Same as in **b** but for 18 ENSO years.

westerly anomalies associated with the northward-propagating counterpart of the early-mid May CMJO trigger the climatological SCS summer monsoon onset.

The above finding then begs the question: how can an equatorial convective disturbance propagate northward? Panels on the right-hand side of Fig. 6a–e depict the zonal mean (110°E–130°E) wet anomalies migrating consistently from 5°S in P25 to about 20°N in P28. During the northward movement of the wet OLR anomalies, the 850-hPa positive (cyclonic) vorticity anomaly generated by the meridional shear of the zonal wind ($-\partial u/\partial y$) is ahead of the propagating convective anomalies. The 850-hPa cyclonic vorticity induces boundary layer convergence and increases the 850-hPa specific humidity, resulting in the northward propagating wet anomalies. The meridional structure of the northward propagating CMJO closely resembles those of the transient northward propagating BSISO over the WNP^{40–42}, suggesting that the boundary layer convergence north of the convective anomaly is a critical environmental condition in driving convective anomaly northward⁴⁰.

The northward propagation theory can be further demonstrated by examining the evolution of the meridional-vertical structure shown in Fig. 7. When the convective anomalies are centered at around 5°S in P24 and P25, the boundary layer convergence is concentrated to the north of the convective anomaly (Fig. 7a, b). Thus, the increased specific humidity in the boundary layer is located north of the convective anomalies, giving rise to a rearward (southward)-tilted moisture distribution most notable in P25 to P27. As a result, the moist lower troposphere becomes more convectively unstable in the north than the south of the convective anomalies, promoting shallow convection ahead of the CMJO and favoring its northward propagation. During P28, the northward propagation stops when

the 850-hPa cyclonic vorticity and specific humidity coincide with the negative OLR anomalies (i.e., no phase lead anymore).

How, then, is the Maritime Continent convective anomaly initiated during P24 and P25? The anomalous winds shown in Fig. 6a, b suggest that the initial convective anomaly over Indonesia is likely influenced by the dry anomalies to its north and east, which could produce the low-level wind convergence south of the equator. Based on a zonally symmetric atmospheric model, the presence of the ISO dry (wet) anomaly in the Northern Hemisphere monsoon region can create an anomalous meridional overturning circulation, which triggers boundary layer convergence (divergence) and the development of a wet (dry) anomaly in the equatorial Southern (Northern) Hemisphere⁴³.

To validate this theory, we examined the vertical-meridional structure of the CMJO from P24 to P28 (Fig. 7). In P24 and P25, the sinking motion induced by the Philippines suppressed convection (15°N–20°N) and generated anomalous southward flows that decrease equatorward ($\partial v/\partial y < 0$), producing boundary layer moisture convergence in the equatorial region and thereby supporting the development of deep convection there. Thus, the theory explains why in P24 and P25, the dry anomalies over the northern Philippines could induce the development of the wet anomalies over Indonesia. Likewise, in P28, the wet SCS anomaly could initiate the dry anomaly over Indonesia subsequently (Figs. 6e and 7e). This type of Asian monsoon-equatorial convective interaction occurs regularly over the eastern Indian Ocean during the boreal summer. When the Indian monsoon is in its peak wet phase, the meridional circulation induces strong downward motions in the equatorial eastern Indian Ocean, which further generates anomalous easterlies that decrease westward, causing low-level convergence in the central equatorial Indian Ocean around 60°E; the latter reinitiate new convection that moves eastward and

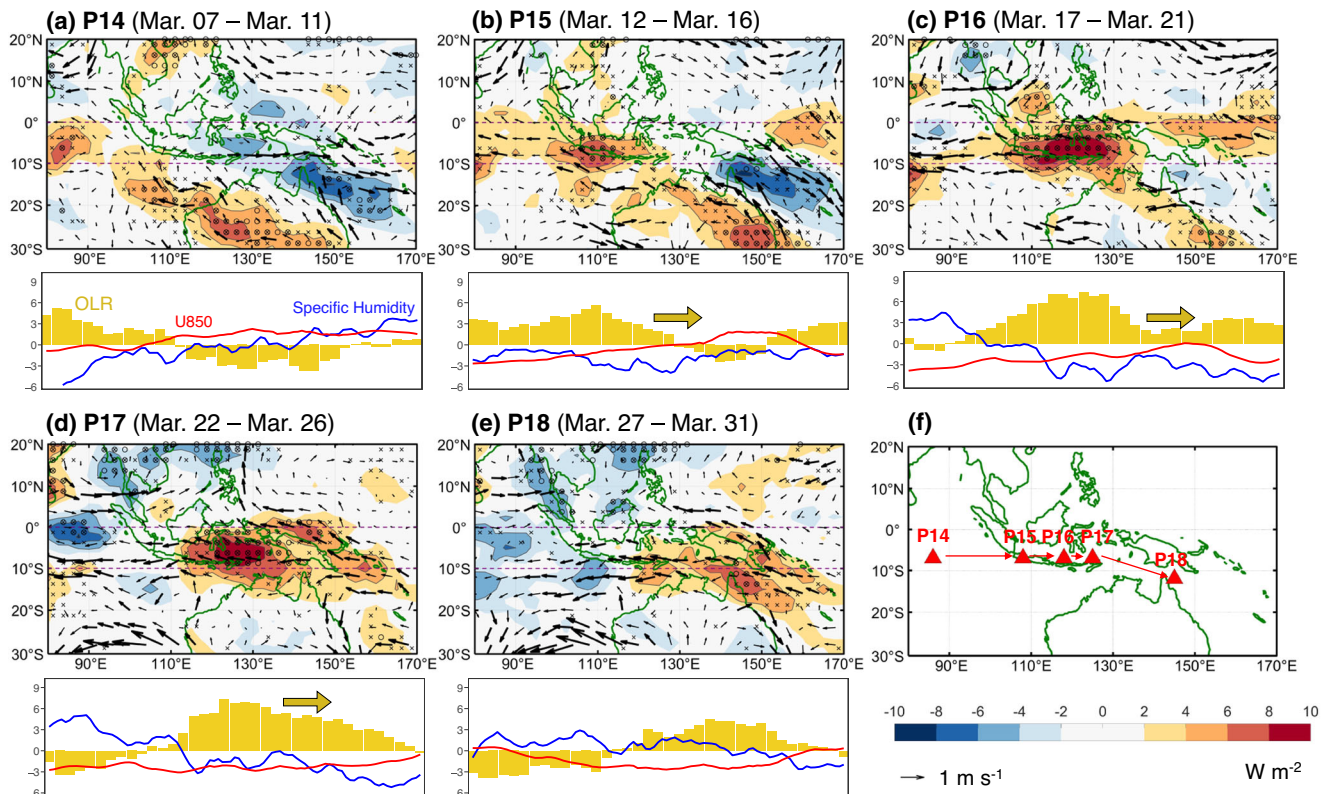


Fig. 5 The CMJO episode linking to the Australian monsoon retreat. Upper panels: OLR (shading, units in W m^{-2}) and 850-hPa winds (vector, bold vectors indicate the wind speed $(u^2 + v^2)^{1/2} > 0.5 \text{ m s}^{-1}$, units in m s^{-1}). The gray cross (circle) indicates a significant CMJO by the A/S (sign) test at the 95% confidence level. Lower panels: Longitudinal structures of the CMJO OLR (yellow bar) and 850-hPa zonal winds (red line, units in 5 m s^{-1}), and 850-hPa specific humidity (blue line, units in 30 g kg^{-1}). All variables are averaged over 10°S to EQ (purple dashed lines). Yellow thick arrows indicate the propagation direction of the OLR CISO signal from (a) P14 to (e) P18. **f** Red triangles and arrows indicate the centroids and propagation direction of the dry CMJO signal from P14 to P18, respectively.

kickstarts the next BSISO cycle, suggesting a self-induction mechanism for maintaining ISM ISO⁴⁴.

The May northern Indian Ocean CMJO and the pre-monsoon drought and ISM burst

Over the northern Indian Ocean, another May CMJO cycle leads to pre-monsoon drought and abrupt ISM burst (Fig. 8). In P24, a dry anomaly, coupled with a low-level anticyclonic anomaly, emerges off the coast of northeast Somalia, followed by an intensification and slow northeastward expansion and migration from P25 to P27 (Fig. 8a–d). In P28, the dry anomaly moves northeastward and rapidly expands from P29 to P30, contributing to the pre-monsoon drought over the Indian subcontinent in late May (Fig. 8e–g). Shortly afterward, a wet spell emerges off Somalia (5°N – 10°N , 55°E – 65°E) during P28 and P29, then moves northeastward toward the Indian subcontinent (Fig. 8e, f). It reaches the southern tip of India in P31 and extends to south of 20°N over the Indian subcontinent (Fig. 8h, i). The landfall timing (i.e., P31) of the wet CMJO phase is highly consistent with the climatological onset date of ISM⁴⁵.

The propagation of the CMJO then explains the teleconnection of the ISM onsets in various places (e.g., Kerala, Bombay, and Calcutta) of the Indian subcontinent (Supplementary Fig. 1). From P27 to P30 (May 11 to May 30), a pre-monsoon dry phase occurs first in Kerala in P28, then in Bombay in P29 and finally in Calcutta in P30 (Supplementary Fig. 1). Following this pre-monsoon dry singularities, a peak wet phase occurs in Kerala and Bombay from P31 to P32 and later in Calcutta from P33 to P34. After P32, not only the three places but the entire Indian subcontinent is occupied by a wet CMJO phase and cyclonic circulation (figure not

shown), which is commensurate with the grand commencement of the ISM based on observations⁴⁶.

DISCUSSION

This work identified three significant CMJO episodes during the boreal spring, which link to the Indonesian–Australian monsoon retreat in mid-March, the SCS (or EA) monsoon onset in mid-May, and the ISM onset in early June. The sudden Australian monsoon retreat results from an equatorial eastward propagation of a dry CMJO originated in the central Indian Ocean. The SCS monsoon onset links to a northward and eastward propagating CMJO initiated in Indonesia. A northeastward propagating wet CMJO arising from Somalia’s off-coast leads to the ISM onset. Before that, the northeastward propagating dry CMJO in May triggers the pre-monsoon drought and heatwaves over India. The CMJO convection and circulation exhibit dynamically coherent structures, supporting its robustness as a convectively coupled circulation system.

The similarities in the dynamic structures and propagation patterns between the transient MJO and CMJO imply that the CMJO may originate from a phase-lock of the transient MJOs to a particular time of the annual cycle. To support this claim, we show how the March CMJO episode is associated with transient MJOs in each year (Fig. 9). The March CMJO exhibits an eastward propagation of dry anomaly from 100°E to 140°E during P15–P18 (Fig. 9a). To find out the dominant propagation patterns in individual years, we adopted the Self-Organizing Map analysis to classify each year’s propagation pattern from 1979 to 2020 and obtained two dominant patterns that both show eastward propagation (Fig. 9b, c). SOM cluster 1, representing 19 years,

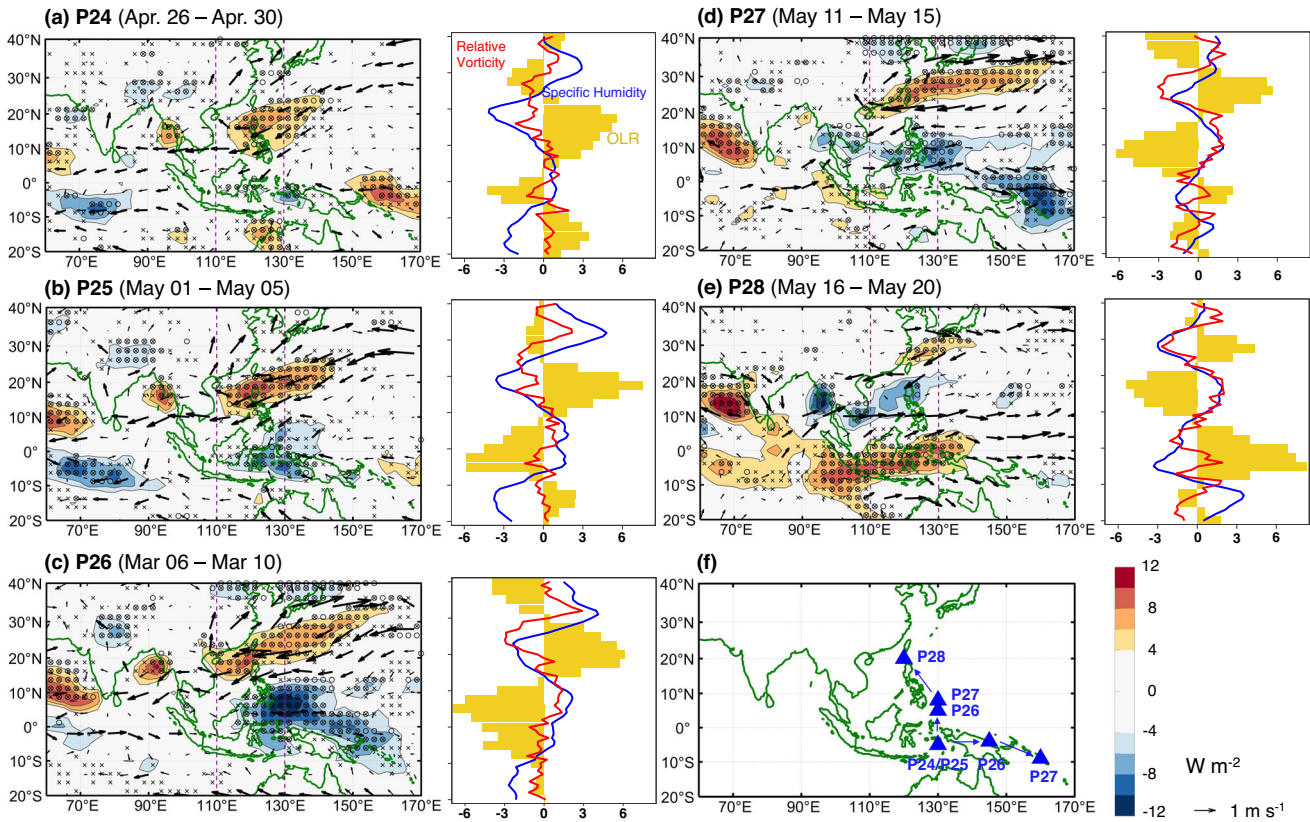


Fig. 6 The CMJO episode triggering the SCS summer monsoon onset. Left panels: The same as in the upper panels in Fig. 5. Right panels: meridional structures of the OLR (yellow bar, units in $W m^{-2}$), 850-hPa relative vorticity (red line, units in $10^6 s^{-1}$), and 850-hPa specific humidity (blue line, units in $10^6 g kg^{-1}$). All variables are averaged over $110^{\circ}E$ - $130^{\circ}E$ from (a) P24 to (e) P28. **f** Blue triangles and arrows indicate the centroids and propagation direction of the wet CMJO signal from P24 to P28, respectively.

shows an eastward propagating dry phase delayed by one pentad compared to the March CMJO (Fig. 9a, b). On the other hand, SOM cluster 2 shows an eastward propagation earlier than the climatological case by about one pentad (Fig. 9a, c). The results suggest that the phase-lock of the transient MJO can produce the CMJO. While the transient MJOs are not precisely in phase with the CMJO, the phase differences are mostly within plus and minus one pentad. As such, the nonlinear interaction between the internal atmospheric variability (MJO) and the insolation-forced annual cycle may explain the origins of the sudden withdrawal of the Australian summer monsoon in late March and the abrupt onset of the Asian monsoon in mid-May to early June.

We have shown that boreal CMJO episodes serve as an atmospheric bridge for the extreme wet and dry phases in the three regional monsoon systems. The Indonesian-Australian monsoon retreat corresponds to a SCS peak wet phase. The SCS summer monsoon onset concurs with the pre-monsoon droughts in the Indian subcontinent, leading the ISM onset by about 15 days. During the ISM onset period, the Australian monsoon experiences a significantly dry period. While the connections among the three regional monsoons of the Asian-Australian monsoon system have been discussed on the seasonal and interannual time scales^{47–50}, our work confirms the existence of the intraseasonal CMJO and its intrinsic role in the three regional monsoon teleconnections. The teleconnections in the peak phases of the three episodes do not mean that the evolutions of these episodes are related because the three CMJO episodes originate from different locations and times and exhibit different propagation paths. The teleconnections manifest the “instantaneous” linkages between the CMJO’s peak precipitation anomaly-induced

heat sources (or sinks) and the atmospheric circulations and convective anomalies.

Predicting monsoon onset, peak, and withdrawal has profound implications on socio-economic activity and natural disaster management^{51,52}. In this respect, the CMJO delivers a source of predictability for subseasonal-to-seasonal (S2S) forecasts, as we have shown that monsoon onset (retreat) typically occurs when hit by a significant wet (dry) phase of CMJO. Successful simulation of the S2S monsoon variabilities may depend on accurate representation of physical processes governing the phase-locked CMJO in the annual cycle. A better understanding of the CISO and its relationship with the monsoon life cycle can advance our knowledge of the source of the S2S predictability and improve weather and climate predictions. The model deficiencies in simulating CISO are intricately linked to the biases in the models’ mean state, including an earlier onset of the SCS summer monsoon with the absence of the CISO signals south of $10^{\circ}N$ ⁵³. On the other hand, the multi-model ensemble mean of the Coupled Model Intercomparison Project Phase 6 (CMIP6) models could well reproduce strong CISOs over the ISM region, the Bay of Bengal, the SCS, and the EA region, although the simulated intensity is weaker, and the peak wet phases are two to three pentads later than the observed⁵⁴. Climate models’ capability in simulating and predicting CISO and the abrupt monsoon transition remains ample room for improvement^{55–58}.

For a long time, the local climate singularity was considered a statistical maneuver until the January Thaw² (a regular recurrence of warming in the mid-winter in New England around the 20th of January that melts snow) links to large-scale circulation⁵⁹. Establishing the linkage between a local singularity and large-scale circulations is fundamental for identifying climate

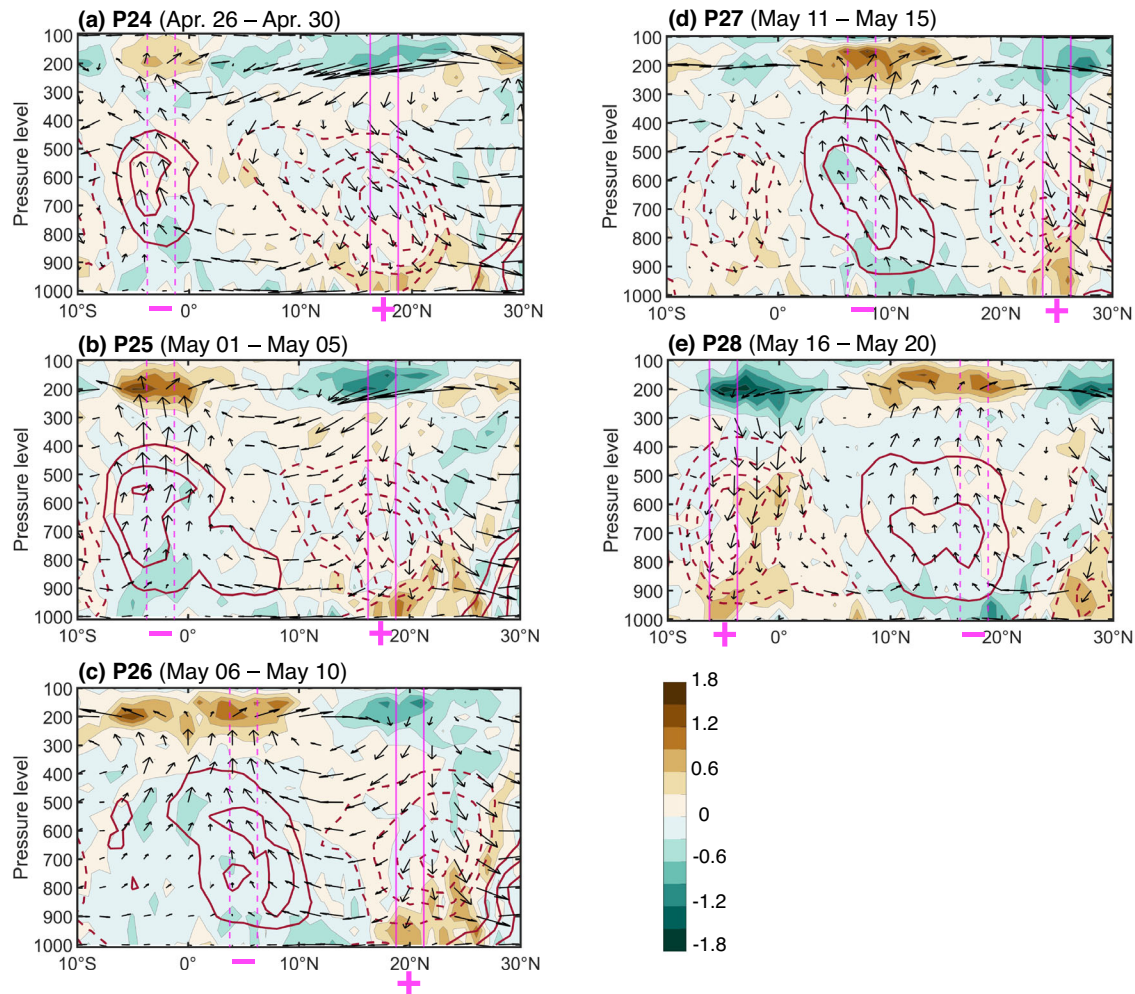


Fig. 7 Vertical-meridional structure of the CMJO averaged over 110°E to 130°E. Shown are the specific humidity [contour, solid (dashed) line for positive (negative) value from 1 to 5 (–5 to –1) with an interval of 1, units in 10^6g kg^{-1}], divergence (shading, units in 10^6s^{-1}), meridional winds and vertical velocity (vector, units in m s^{-1} and 10^2Pa s^{-1}). The purple dashed (solid) lines with plus (minus) signs represent the latitudinal range of the maximum (minimum) OLR CMJO from (a) P24 to (e) P28.

singularities. The present work provides an observational footing for attributing the boreal spring Asian-Australian monsoon singularities to the MJO's phase-locking to the annual cycle.

It should be noted that CISO is generally a nonstationary phenomenon. Through examining a 227-year daily precipitation record gathered in Seoul, South Korea, the characteristics of the rainy season, including the dates of onset, retreat, and summit, exhibit significant centennial variations, indicating the time-varying monsoon singularities detected by a 30-yr climatology change with time¹⁴. Based on rainfall data from 1951 to 2004, it was found that the regime shift of CISO occurred over the Indian subcontinent around mid-1970, related to the change in the northward propagation speed of CISO⁶⁰. Nevertheless, the CISO non-stationarity is not a surprise because the climatology defined by a 30-year mean state generally changes with time due to external forcings, such as solar orbital forcing, solar irradiance cycles, volcanos aerosols, and internal dynamics within the coupled climate system, such as multidecadal variability in the Atlantic and Pacific oceans. Future studies of the secular changes in CISO and monsoon singularity will help better understand the cause of climate change.

Note also that the magnitude of the OLR CISO signal over the Arabian Sea region is two to three times larger than other monsoon regions (Fig. 2). In particular, the strong negative OLR CISO in P32 and

P33 (June 5 to June 14) heralds the peak rainy season over the Arabian Sea (Fig. 1). The interannual variability of ISO linked to ENSO is significantly weaker over the Arabian Sea than the SCS¹³. Moreover, compared with the WNP, the ISO in the Arabian Sea and Indian monsoon region is less sensitive to the change of summer mean state⁶¹. This implies that the local ocean-atmosphere interaction on a subseasonal time scale could be a critical factor in the Arabian Sea and the northern Indian Ocean⁴¹, which may be associated with the development of the localized ISO. It was argued that the tight phase lock of ISO to the annual cycle over this region is likely attributed to the modulation of ISO by the large-scale circulation that is driven by the punctuated annual warming of the Indian subcontinent and northern Indian Ocean⁶². However, what fundamentally determines the timing and locations of the ISO's phase-locking remains to be investigated.

METHODS

Data

The daily mean OLR data is retrieved from the NOAA Interpolated OLR dataset for the 42 years from 1979 to 2020⁶³. All other daily data of various meteorological variables are retrieved from the fifth generation of the European Centre for Medium-Range

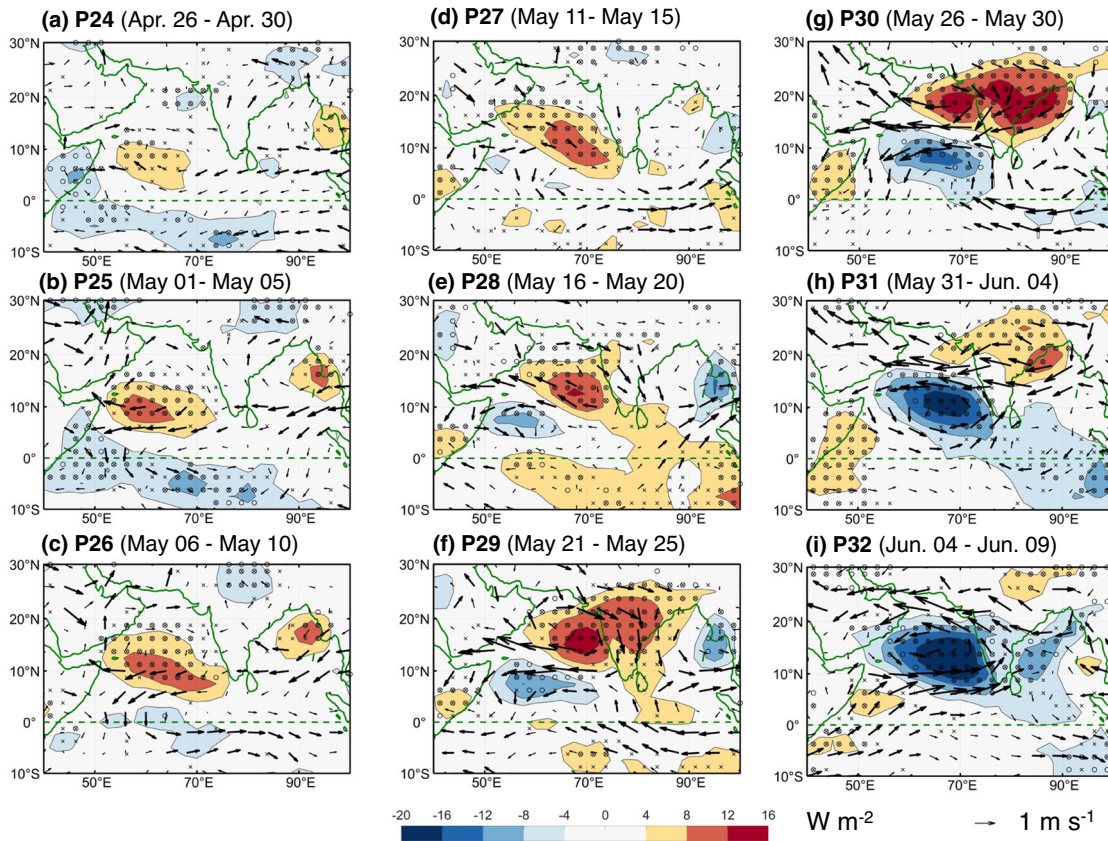


Fig. 8 The CMJO episode triggers the ISM burst. Similar to the upper panels of Fig. 5, but for the Indian Ocean basin from (a) P24 to (i) P32.

Weather Forecasts (ECMWF) reanalysis data (ERA5) at 1° longitude \times 1° latitude horizontal resolution over 1979–2020⁶⁴.

Definition of CISO

To detect the CISO signals, we decomposed the climatological pentad-mean time series of a particular variable $[X_c(i), i = 1, \dots, 73]$ into three components by Fourier harmonic analysis⁶:

$$X_c(i) = X_{ca}(i) + X_{ciso}(i) + R(i), \quad (1)$$

where i denotes Julian P1 to P73, X_{ca} denotes the slow annual cycle defined by the sum of the first four Fourier harmonics (period ranging from three months to a year), X_{ciso} represents the CISO captured by the sum of the 5th to 18th harmonics (periods ranging from 20 to 73 days), and R is the residual.

Supplementary Fig. 2a shows an example of the climatological pentad mean OLR and its CISO component at a location of the central Maritime Continent (5°S , 120°E). The CISO consistently shows three conspicuous positive signals peak (i.e., monsoon singularities) at early January (P3), mid-March (P16), and mid-May (P28), indicating salient dry anomalies from the slow annual cycle.

Statistical significance of CISO

The prominent positive or negative OLR CISO signals in Indonesia (5°S , 120°E), shown in Supplementary Fig. 2a, tend to occur at some specific pentads. Here we adopted two rudimental statistical significance tests to assess whether the CISO is statistically significant following WX97⁶.

The sign test examines the probability of a positive (or negative) anomaly event for 42 years. The null hypothesis is that a negative (or positive) anomaly occurs randomly at any given pentad with a 50% probability of occurrence. We use the number of occurrences of negative (or positive) anomalies observed in the 42 years to

make a maximum likelihood estimation of the probability⁶⁵. Whenever 50% falls out of the 95% confidence interval of the estimated probability (in this case, greater than or equal to 26 occurrences in 42 years), the null hypothesis is rejected at the 0.05 significance level. Supplementary Fig. 2b displays the number of wet (i.e., negative OLR anomaly) and dry (i.e., positive OLR anomaly) episodes at each pentad obtained from the OLR anomaly of each year at (5°S , 120°E). During P18–P24, positive or negative OLR anomaly occurs randomly. Thus, the occurrence of negative or positive events is not significantly biased. However, greater than or equal to 26 dry (wet) events occur during P15–P17 and P28–P29 (P25–P26), indicating that the CMJO signals during those pentads significantly differ from the normal climatology, thus referring to significant dry (wet) CMJO signals.

The Amplitude/Standard Deviation (A/S) ratio test compares the amplitude of CISO with its year-to-year variability (interannual standard deviation). The null hypothesis of the A/S test is that the observed sample means (the amplitude) at a fixed pentad is from a population characterized by zero mean (i.e., the amplitude at a fixed pentad is not significantly different from zero). The Student's t -statistic applied to this test writes

$$t = \frac{A}{(S/\sqrt{n})}, \quad (2)$$

where A is the CMJO amplitude at a particular pentad, S is the standard deviation (sample spread) at that given pentad, computed from the interannual variability of the variable's anomaly, and n is the sample size (i.e., 42). The critical t -value with $n-1$ (41) degrees of freedom is 1.68 and 2.20 at the 90% and 95% confidence levels, respectively. Consequently, the null hypothesis can be rejected at the 95% confidence level if $t > 2.20$ (i.e., $A/S > 0.31$), implying that the CISO cannot be viewed as an ordinary sampling fluctuation. Supplementary Fig. 2c and

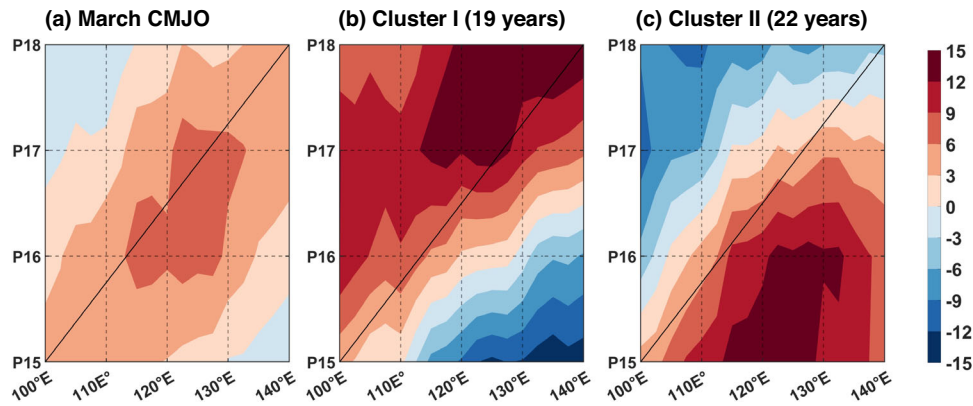


Fig. 9 Linkage between the March CMJO and the transient MJOs each year. Longitude-time diagram of the OLR anomalies averaged between 0° and 10°S in **a** 42 years (1979–2020), **b** 19 years of cluster I events, and **c** 22 years of cluster II events.

Supplementary Fig. 3 exhibit the A/S ratio. Notice that in the Supplementary Fig. 2c, the A/S ratio exceeds 0.6 in P28, indicating a highly significant, phase-locked CMJO signal. The A/S test yields generally consistent results with the sign test.

DATA AVAILABILITY

The meteorological data is retrieved from the ERA5 by the European Center for Medium-Range Weather Forecast (ECMWF) at <https://www.ecmwf.int/en/forecasts/datasets/reanalysis-datasets/era5>. The daily mean Outgoing Longwave Radiation data is retrieved from the NOAA Interpolated OLR dataset at <https://psl.noaa.gov/data/gridded/data.olrcdr.interp.html>. Derived data supporting the findings of this study are available from the corresponding author upon reasonable request.

CODE AVAILABILITY

The source codes for the analysis of this study are available from the corresponding authors upon reasonable request.

Received: 11 September 2023; Accepted: 2 January 2024;

Published online: 07 February 2024

REFERENCES

- Wang, B., Liu, J., Kim, H. J., Webster, P. J. & Yim, S. Y. Recent change of the global monsoon precipitation (1979–2008). *Clim. Dyn.* **39**, 1123–1135 (2012).
- Wahl, E. W. Singularities and the general circulation. *J. Meteorol.* **10**, 42–45 (1953).
- Lanzante, J. R. Some singularities and irregularities in the seasonal progression of the 700 mb height field. *J. Clim. Appl. Meteor.* **22**, 967–981 (1983).
- Wang, B., LinHo, Zhang, Y. & Lu, M. M. Definition of South China sea monsoon onset and commencement of the East Asia summer monsoon. *J. Clim.* **17**, 699–710 (2004).
- Joseph, P. V., Sooraj, K. P. & Rajan, C. K. The summer monsoon onset process over South Asia and an objective method for the date of monsoon onset over Kerala. *Int. J. Climatol.* **26**, 1871–1893 (2006).
- Wang, B. & Xu, X. Northern hemisphere summer monsoon singularities and climatological intraseasonal oscillation. *J. Clim.* **10**, 1071–1085 (1997).
- Madden Roland, A. & Julian Paul, R. Description of global-scale circulation cells in the tropics with a 40–50 day period. *J. Atmos. Sci.* **29**, 1109–1123 (1972).
- Wang, B. & Xie, X. A model for the boreal summer intraseasonal oscillation. *J. Atmos. Sci.* **54**, 72–86 (1997).
- Suhas, E., Neena, J. M. & Goswami, B. N. An Indian monsoon intraseasonal oscillations (MISO) index for real time monitoring and forecast verification. *Clim. Dyn.* **40**, 2605–2616 (2013).
- Kang, I.-S., Ho, C.-H., Lim, Y.-K. & Lau, K.-M. Principal modes of climatological seasonal and intraseasonal variations of the Asian Summer Monsoon. *Mon. Wea. Rev.* **127**, 322–340 (1999).
- Wu, R. & Wang, B. Multi-stage onset of the summer monsoon over the western North Pacific. *Clim. Dyn.* **17**, 277–289 (2001).
- LinHo & Wang, B. The time-space structure of the Asian-Pacific Summer Monsoon: a fast annual cycle view*. *J. Clim.* **15**, 2001–2019 (2002).
- Kajikawa, Y. & Yasunari, T. Interannual variability of the 10–25- and 30–60-day variation over the South China Sea during boreal summer. *Geophys. Res. Lett.* **32**, 1–4 (2005).
- Wang, B., Jhun, J. G. & Moon, B. K. Variability and singularity of Seoul, South Korea, Rainy Season (1778–2004). *J. Clim.* **20**, 2572–2580 (2007).
- Goswami, B. N. South Asian Monsoon, Intraseasonal Variability of the Atmosphere-Ocean Climate System. (eds. Lau W. K. M. & Waliser D. E.) (Springer, 2011).
- Song, Z., Zhu, C., Su, J. & Liu, B. Coupling modes of climatological intraseasonal oscillation in the East Asian summer monsoon. *J. Clim.* **29**, 6363–6382 (2016).
- Chu, J. E., Wang, B., Lee, J. Y. & Ha, K. J. Boreal summer intraseasonal phases identified by nonlinear multivariate empirical orthogonal function-based self-organizing map (ESOM) analysis. *J. Clim.* **30**, 3513–3528 (2017).
- Li, J., Liu, B. & Mao, J. Climatological intraseasonal oscillation in the middle-upper troposphere and its effect on the northward migration of the East Asian westerly jet and rain belt over eastern China. *Int. J. Climatol.* **41**, 5084–5099 (2021).
- Kikuchi, K., Wang, B. & Kajikawa, Y. Bimodal representation of the tropical intraseasonal oscillation. *Clim. Dyn.* **38**, 1989–2000 (2012).
- Webster, P. J. & Yang, S. Monsoon and ENSO: selectively interactive systems. *Q. J. R. Meteorol. Soc.* **118**, 877–926 (1992).
- Wang, B. & Fan, Z. Choice of South Asian summer monsoon indices. *Bull. Am. Meteorol. Soc.* **80**, 629–638 (1999).
- Goswami, B. N., Krishnamurthy, V. & Annamalai, H. A broad-scale circulation index for the interannual variability of the Indian summer monsoon. *Q. J. R. Meteorol. Soc.* **125**, 611–633 (1999).
- Wang, B. et al. How to measure the strength of the East Asian summer monsoon. *J. Clim.* **21**, 4449–4463 (2008).
- Dai, L., Cheng, T. F. & Lu, M. Define East Asian monsoon annual cycle via a self-organizing map-based approach. *Geophys. Res. Lett.* **48**, e2020GL089542 (2021).
- Kajikawa, Y., Wang, B. & Yang, J. A multi-time scale Australian monsoon index. *Int. J. Climatol.* **30**, 1114–1120 (2010).
- Wang, B., Ding, Q. & Joseph, P. V. Objective definition of the Indian summer monsoon onset. *J. Clim.* **22**, 3303–3316 (2009).
- Dai, L., Cheng, T. F., Wang, B. & Lu, M. The Subseasonal Features of Indian Monsoon. *J. Clim.* (2023).
- Waliser, D. E. Intraseasonal Variability. In *The Asian Monsoon* (ed. Wang, B.) 585–612 (Springer-Praxis, Berlin, 2006).
- Rasmusson, E. M. & Carpenter, T. H. Variations in tropical sea surface temperature and surface wind fields associated with the Southern Oscillation/El Niño. *Mon. Wea. Rev.* **110**, 354–384 (1982).
- An, S.-I. & Wang, B. Interdecadal change of the structure of the ENSO mode and its impact on the ENSO frequency. *J. Clim.* **13**, 2044–2055 (2000).
- Hendon, H. H., Zhang, C. & Glick, J. D. Interannual variation of the Madden-Julian Oscillation during Austral Summer. *J. Clim.* **12**, 2538–2550 (1999).
- Wang, B., Chen, G. & Liu, F. Diversity of the Madden-Julian Oscillation. *Sci. Adv.* **5**, eaax0220 (2019).
- Zhang, S. & Wang, B. Global summer monsoon rainy seasons. *Int. J. Climatol.* **28**, 1563–1578 (2008).
- Hendon, H. H. & Liebmann, B. The Intraseasonal (30–50 day) Oscillation of the Australian Summer Monsoon. *J. Atmos. Sci.* **47**, 2909–2923 (1990).
- Wang, B., Liu, F. & Chen, G. A trio-interaction theory for Madden-Julian oscillation. *Geosci. Lett.* **3**, 34 (2016).
- Kemball-Cook, S. & Wang, B. Equatorial waves and air-sea interaction in the boreal summer intraseasonal oscillation. *J. Clim.* **14**, 2923–2942 (2001).

37. Lee, S. S. & Wang, B. Regional boreal summer intraseasonal oscillation over Indian ocean and western pacific: comparison and predictability study. *Clim. Dyn.* **46**, 2213–2229 (2016).
38. Xie, A., Chung, Y.-S., Liu, X. & Ye, Q. The interannual variations of the summer monsoon onset over the South China Sea. *Theor. Appl. Climatol.* **59**, 201–213 (1998).
39. Shao, X., Huang, P. & Huang, R. H. Role of the phase transition of intraseasonal oscillation on the South China Sea summer monsoon onset. *Clim. Dyn.* **45**, 125–137 (2015).
40. Hsu, H.-H., Weng, C.-H. & Wu, C.-H. Contrasting characteristics between the Northward and Eastward propagation of the intraseasonal oscillation during the boreal summer. *J. Clim.* **17**, 727–743 (2004).
41. Wang, B., Webster, P., Kikuchi, K., Yasunari, T. & Qi, Y. Boreal summer quasi-monthly oscillation in the global tropics. *Clim. Dyn.* **27**, 661–675 (2006).
42. Chen, G. & Wang, B. Diversity of the boreal summer intraseasonal oscillation. *J. Geophys. Res. Atmos.* **126**, e2020JD034137 (2021).
43. Drbohlav, H.-K. L. & Wang, B. Mechanism of the Northward-propagating intraseasonal oscillation: insights from a zonally symmetric model. *J. Clim.* **18**, 952–972 (2005).
44. Wang, B., Webster, P. J. & Teng, H. Antecedents and self-induction of active-break south Asian monsoon unraveled by satellites. *Geophys. Res. Lett.* **32**, 1–4 (2005).
45. Joseph, P. V., Eischeid, J. K. & Pyle, R. J. Interannual variability of the onset of the Indian summer monsoon and its association with atmospheric features, El Niño, and sea surface temperature anomalies. *J. Clim.* **7**, 81–105 (1994).
46. Fasullo, J. & Webster, P. J. A hydrological definition of Indian Monsoon onset and withdrawal. *J. Clim.* **16**, 3200–3211 (2003).
47. Matsumoto, J. The seasonal changes in Asian and Australian. *Monsoon Reg. J. Meteorol. Soc. Jpn* **70**, 257–273 (1992).
48. Meehl, G. A. & Arblaster, J. M. The tropospheric biennial oscillation and Asian-Australian monsoon rainfall. *J. Clim.* **15**, 722–744 (2002).
49. Kripalani, R. H. & Kulkarni, A. Monsoon rainfall variations and teleconnections over South and East Asia. *Int. J. Climatol.* **21**, 603–616 (2001).
50. He, J., Sun, C., Liu, Y., Matsumoto, J. & Li, W. Seasonal transition features of large-scale moisture transport in the Asian-Australian monsoon region. *Adv. Atmos. Sci.* **24**, 1–14 (2007).
51. Gadgil, S. & Rupa Kumar, K. The Asian monsoon-agriculture and economy. In *The Asian Monsoon* (ed. Wang, B.) 844 (Springer, 2006).
52. Dai, L., Cheng, T. F. & Lu, M. Anthropogenic warming disrupts intraseasonal monsoon stages and brings dry-get-wetter climate in future East Asia. *npj Clim. Atmos. Sci.* **5**, 1–10 (2022).
53. Yang, J., Wang, B. & Li, L. The East Asia-western North Pacific boreal summer intraseasonal oscillation simulated in GAMIL 1.1.1. *Adv. Atmos. Sci.* **26**, 480–492 (2009).
54. Wang, H., Liu, F. & Dong, W. Features of climatological intraseasonal oscillation during Asian summer monsoon onset and their simulations in CMIP6 models. *Clim. Dyn.* **59**, 3153–3166 (2022).
55. Waliser, D. E. et al. AGCM simulations of intraseasonal variability associated with the Asian summer monsoon. *Clim. Dyn.* **21**, 423–446 (2003).
56. Sabeerali, C. T. et al. Simulation of boreal summer intraseasonal oscillations in the latest CMIP5 coupled GCMs. *J. Geophys. Res. Atmos.* **118**, 4401–4420 (2013).
57. Neena, J. M., Lee, J. Y., Waliser, D., Wang, B. & Jiang, X. Predictability of the Madden-Julian oscillation in the intraseasonal variability hindcast experiment (ISVHE). *J. Clim.* **27**, 4531–4543 (2014).
58. Lee, S. S., Wang, B., Waliser, D. E., Neena, J. M. & Lee, J. Y. Predictability and prediction skill of the boreal summer intraseasonal oscillation in the Intraseasonal Variability Hindcast Experiment. *Clim. Dyn.* **45**, 2123–2135 (2015).
59. Godfrey, C. M., Wilks, D. S. & Schultz, D. M. Is the January Thaw A statistical phantom? *Bull. Am. Meteorol. Soc.* **83**, 53–62 (2002).
60. Suhas, E. & Goswami, B. N. Regime shift in Indian summer monsoon climatological intraseasonal oscillations. *Geophys. Res. Lett.* **35**, L20703 (2008).
61. Teng, H. & Wang, B. Interannual variations of the boreal summer intraseasonal oscillation in the Asian-Pacific Region. *J. Clim.* **16**, 3572–3584 (2003).
62. Wang, B. & Lin, H. Rainy season of the Asian-Pacific summer monsoon. *J. Clim.* **15**, 386–398 (2002).
63. Liebmann, B. & Smith, C. A. Description of a complete (interpolated) outgoing longwave radiation dataset. *Bull. Am. Meteorol. Soc.* **77**, 1275–1277 (1996).
64. Hersbach, H. et al. The ERA5 global reanalysis. *Q. J. R. Meteorol. Soc.* **146**, 1999–2049 (2020).
65. Johnson, N. L., Kemp, A. W. & Kotz, S. *Univariate Discrete Distributions*. (John Wiley & Sons, Inc., 2005).

ACKNOWLEDGEMENTS

This work is supported by the National Science Foundation of (Climate Dynamics Division Award No. AGS-2025057). SSL was supported by the Institute for Basic Science (IBS), Republic of Korea, under IBS-R028-D1. This is publication No. 11759 of the SOEST, publication No. 1616 of IPRC, and publication No. 416 of Earth System Modeling Center (ESMC).

AUTHOR CONTRIBUTIONS

B.W. conceived, drafted the paper, and supervised the study. All co-authors contributed to computation and figure plotting, drafting and revising the manuscript, or discussion of results.

COMPETING INTERESTS

The authors declare no competing interests.

ADDITIONAL INFORMATION

Supplementary information The online version contains supplementary material available at <https://doi.org/10.1038/s41612-024-00566-9>.

Correspondence and requests for materials should be addressed to Bin Wang or Lun Dai.

Reprints and permission information is available at <http://www.nature.com/reprints>

Publisher's note Springer Nature remains neutral with regard to jurisdictional claims in published maps and institutional affiliations.



Open Access This article is licensed under a Creative Commons Attribution 4.0 International License, which permits use, sharing, adaptation, distribution and reproduction in any medium or format, as long as you give appropriate credit to the original author(s) and the source, provide a link to the Creative Commons license, and indicate if changes were made. The images or other third party material in this article are included in the article's Creative Commons license, unless indicated otherwise in a credit line to the material. If material is not included in the article's Creative Commons license and your intended use is not permitted by statutory regulation or exceeds the permitted use, you will need to obtain permission directly from the copyright holder. To view a copy of this license, visit <http://creativecommons.org/licenses/by/4.0/>.

© The Author(s) 2024